

DIRECT IMAGING CONSTRAINTS ON THE PUTATIVE EXOPLANET 14 Her C*

TIMOTHY J. RODIGAS¹, JARED R. MALES¹, PHILIP M. HINZ¹, ERIC E. MAMAJEK², AND RUSSELL P. KNOX¹

¹ Steward Observatory, The University of Arizona, 933 North Cherry Avenue, Tucson, AZ 85721, USA; rodigas@as.arizona.edu

² Department of Physics & Astronomy, University of Rochester, Rochester, NY 14627-0171, USA

Received 2010 October 13; accepted 2011 February 16; published 2011 April 7

ABSTRACT

We present results of deep direct imaging of the radial velocity (RV) planet-host star 14 Her (=GJ 614, HD 145675), obtained in the L' band with the Clio-2 camera and the MMT adaptive optics system. This star has one confirmed planet and an unconfirmed outer companion, suggested by residuals in the RV data. The orbital parameters of the unconfirmed object are not well constrained since many mass/semimajor axis configurations can fit the available data. The star has been directly imaged several times, but none of the campaigns has ruled out sub-stellar companions. With ~ 2.5 hr of integration, we rule out at 5σ confidence $\gtrsim 18 M_J$ companions beyond ~ 25 AU, based on the Baraffe et al. COND mass–luminosity models. Combining our detection limits with fits to the RV data and analytic dynamical analysis, we constrain the orbital parameters of 14 Her c to be $3 \lesssim m/M_J \lesssim 42$, $7 \lesssim a/\text{AU} \lesssim 25$, and $e \lesssim 0.5$. A wealth of information can be obtained from RV/direct imaging overlap, especially with deep imaging as this work shows. The collaboration between RV and direct imaging will become more important in the coming years as the phase space probed by each technique converges. Future studies involving RV/imaging overlap should be sure to consider the effects of a potential planet’s projected separation, as quoting limits assuming face-on orientation will be misleading.

Key words: planetary systems – stars: individual (14 Her) – techniques: high angular resolution

1. INTRODUCTION

In recent years, several exoplanets have been discovered by direct imaging (Marois et al. 2008; Kalas et al. 2008; Lagrange et al. 2010). While the radial velocity (RV) technique has by far discovered the most exoplanets (525 as of 2011 February, <http://exoplanet.eu>), the few direct imaging discoveries have expanded our knowledge of exoplanets significantly. The directly imaged planet orbiting Fomalhaut (Kalas et al. 2008) shows evidence for having cleared out dusty material in the star’s debris disk. The four ~ 10 Jupiter-mass (M_J) planets in the HR 8799 system (Marois et al. 2008, 2010) orbit at such a wide range of distances that they challenge all current planet formation theories. The Sun-like star GJ 758 has a $\sim 40 M_J$ companion with a $T_{\text{eff}} < 600$ K, making it one of the coldest objects ever discovered (Thalmann et al. 2009; Currie et al. 2010). Recently, direct imaging has helped probe exoplanet atmospheres; Janson et al. (2010) characterized the atmosphere of HR 8799 c via spectra and Hinz et al. (2010) characterized the atmospheres of HR 8799 b, c, and d via photometry at $3\text{--}5 \mu\text{m}$. For the first time significant orbital motion has been imaged for the planet in the β Pic system (Lagrange et al. 2009, 2010). This has helped constrain the planet’s orbit.

While the RV technique is mostly sensitive to planets orbiting close (semimajor axis $a \lesssim 5$ AU) to their host stars, direct imaging probes the outer ($a \gtrsim 5$ AU) regions. Thus, direct imaging and RV complement each other. A star’s planetary system architecture can be fully determined when it is studied by both RV and direct imaging. A planet’s true mass, semimajor axis, eccentricity, and orbital inclination can be determined when it is detected by both RV and direct imaging. Mass–luminosity models for low-mass brown dwarfs and gas-giant planets (e.g., Baraffe et al. 2003; Burrows et al. 2003) can also be constrained and improved in this case.

The optimal targets for direct imaging are young planets on wide orbits. Since the optimal RV targets are old, quiescent stars with close-in planets, the sample of systems that satisfy both techniques’ requirements is currently very small. Even if one cannot currently image any known companions, perhaps imaging of RV stars can detect previously undiscovered companions. Rodigas & Hinz (2009) used Monte Carlo simulations of RV data to show that as many as 15% of RV systems that contain a single, moderately eccentric planet may have an additional massive planet on a wide orbit. In this case, the outer planet’s RV signal is weak enough that it is not detected above the noise. A more favorable case would be if the outer planet was suggested by a long-term trend in the RV data. Then we know the companion is there, and it is just a matter of detecting it.

The star 14 Her (=GJ 614, HD 145675) is a prime target for RV/direct imaging overlap. At a distance of 17.6 ± 0.1 pc (van Leeuwen 2007), it is close enough that direct imaging can probe as close as ~ 9 AU from the star. 14 Her is a multiple-body system. It has one detected planet (of minimum mass $4.64 M_J$, semimajor axis $a = 2.77$ AU, and eccentricity $e = 0.369$) and a second unconfirmed companion that has been suggested by a long-term trend in the RV data (Wittenmyer et al. 2007; Goździewski et al. 2006, 2008). Two-planet Keplerian fits to the data suggest that the outer companion is $\gtrsim 2.1 M_J$ and orbits at $\gtrsim 7$ AU (Wittenmyer et al. 2007). Dynamical analysis by Goździewski et al. (2008) suggests a best-fit, minimum χ^2 mass of $\sim 8 M_J$ and a semimajor axis of ~ 9 AU, though there were a host of low- χ^2 solutions. Figure 1 shows the current RV data excluding the orbit of the primary from Wittenmyer et al. (2007). Due to the lack of data covering the orbit of the outer companion, there are many different possible mass/semimajor axis solutions.

The companion, at a minimum, orbits on a fairly wide orbit. This is beneficial for direct imaging since luminous objects on wide orbits are easier to detect via imaging than objects

* Observations reported here were obtained at the MMT Observatory, a joint facility of the University of Arizona and the Smithsonian Institution.

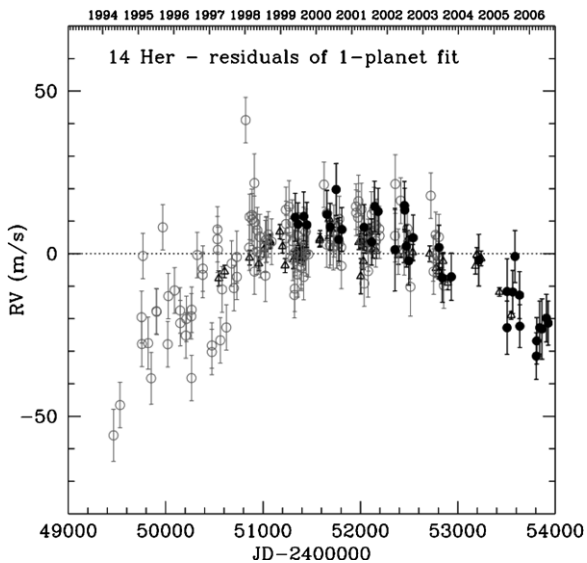


Figure 1. RV data excluding the primary (b) component for 14 Her, from Wittenmyer et al. (2007). Because the observation baseline is shorter than the companion’s long period, there are many possible good fits to the data and therefore many possible values for 14 Her c’s mass, semimajor axis, and eccentricity.

on small orbits. This comes from imaging typically having better contrast (and therefore sensitivity) farther from the star. Imaging, especially at the current epoch, is also favorable given that for most of the possible orbital solutions 14 Her c is likely to have a large projected separation; only for some high inclination solutions can the planet be behind or in front of the star.

Direct imaging of stars with known exoplanets has yielded strong constraints on planetary masses orbiting at large separations (e.g., Janson et al. 2009; Heinze et al. 2008; Kenworthy et al. 2009). With regard to 14 Her, there have been several direct imaging campaigns. Two direct imaging campaigns with the Keck and Lick Observatories have already ruled out stellar-mass ($M > 80 M_J$) companions beyond 9 and 12.7 AU, respectively (Luhman & Jayawardhana 2002; Patience et al. 2002).³ Carson et al. (2009) used the Palomar telescope to rule out $\sim 70 M_J$ companions beyond ~ 18 AU.³ Recently, Leconte et al. (2010) used the Advanced Electro-Optical System telescope to conduct an imaging survey of nearby solar-like stars, one of which was 14 Her. However, with only ~ 20 minutes of integration they do not report any significant detection limits for this star. Deeper imaging is required to set meaningful constraints on 14 Her c and any other potential companions.

To investigate the nature of 14 Her c and probe for additional high-mass planets and brown dwarfs, we have carried out deep direct imaging of 14 Her in the L' band with the MMT adaptive optics (AO) system. In Section 2 we describe the observations and data reduction. In Section 3 we present our constraints on 14 Her c’s mass, combining analysis of the published RV data with our direct imaging results and analytic dynamical analysis. In Section 4 we summarize and conclude.

2. OBSERVATIONS AND DATA REDUCTION

Observations were carried out at the MMT on Mount Hopkins in Arizona on the night of UT 2010 May 30. We used Clio-2 (Freed et al. 2004; Sivanandam et al. 2006; Hinz et al. 2006; Currie et al. 2010), Arizona’s high-contrast near-infrared

camera and observed in the L' band. The field of view was approximately $9''$ by $30''$, with a plate scale of $29.9 \text{ mas pixel}^{-1}$, determined by observations of the binary star HD 223718. We turned the instrument rotator off so that the field of view would rotate throughout the observations; this is essential for high-contrast angular differential imaging (ADI; Marois et al. 2006). Observing conditions were optimal, with clear skies, good seeing, and the AO providing consistently good atmospheric correction. Throughout the observations, we nodded the telescope every few minutes by $10''$ so that each image would contain the target star and sky background. We obtained 8764.7 s (2 hr 26 minutes) of integration on 14 Her. At $\sim 50\%$ efficiency with Clio-2 in the L' band, this translated into ~ 5 hr of wall-clock time. A small fraction of the obtained images were not used in the data reduction due to the AO being off, wind shake distorting the star, or an infrequent occurrence of losing the star on separate telescope nods. We also obtained unsaturated images of 14 Her and HD 203856 (an L' standard star from Leggett et al. 2003) using a neutral density filter to calibrate our photometry.

Images were saved and written as stacked data cubes. All data reduction was performed with custom scripts in Matlab. We divided each image by the number of frames in each data cube and by the integration time to produce units of dn s^{-1} for each pixel. We corrected the images for bad pixels using a bad pixel mask, and we removed detector and image artifacts as follows: since each image serves as both a target image and a background image, each image was subtracted from the opposite-nod image obtained closest in time to it, as long as that image had not already been used in the nod-subtraction process. Once an image is used to remove sky background, it is no longer available for nod-subtraction. Since we saturated the central $0''.3$ core of the star in each image, we determined the pixel location of the star by smoothing each image with a 25 pixel ($0''.75$) disk (pillbox) average, finding the maximum pixel location, then calculating the center of light at this pixel within a $0''.75$ radius. Calculating the center of light allows for sub-pixel registration, which increases contrast. We used the center of light location to register each nod-subtracted image to a common pixel location. We then reduced the images using the LOCI algorithm (Lafrenière et al. 2007). Each image was rotated clockwise by $2^\circ 53'$ minus its parallactic angle to obtain north up and east left. The $2^\circ 53'$ rotational constant was determined by observing the binary star HD 223718. The final image was produced by median-combining the set of all the images. The change in parallactic angle between the first and last images taken during the night was 158° , allowing us to detect point sources all the way up to the saturated central star ($0''.3$).

3. RESULTS AND DISCUSSION

Figure 2 shows our final reduced image of 14 Her. No candidate companions are identified. Some point sources masquerade as “real,” but after dividing up the data into the first and second half of the night, all sources can be ruled out as speckles.

To determine our sensitivity level, we calculated the standard deviation per pixel in a 5 pixel ($0''.15 = \text{FWHM}$) annulus centered on the star, from $0''.3$ to $2''$. We compared the total flux in a 5 pixel aperture centered on the unsaturated image of HD 203856 to the 14 Her standard deviation per pixel \times the square root of the number of pixels in the 5 pixel aperture. We used this ratio to calculate the apparent magnitude of the 14 Her background as a function of separation from the star. We used unsaturated images of 14 Her to calculate its apparent magnitude relative to the standard star HD 203856. We calculated this value

³ These limits assume a face-on orientation to the star, which is unlikely.

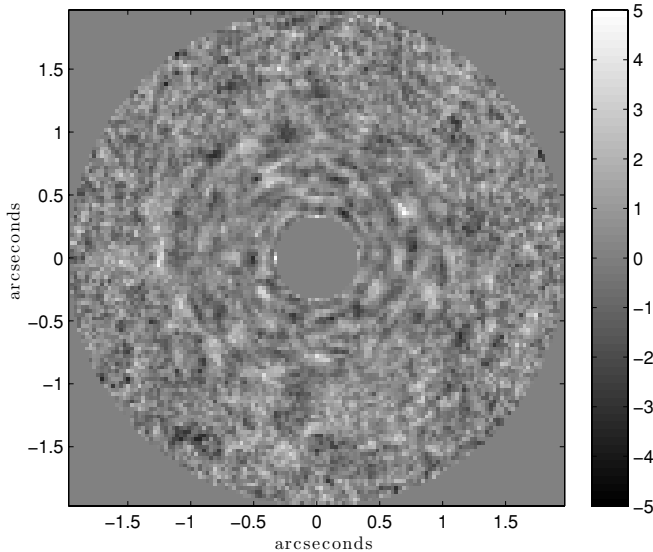


Figure 2. Final reduced image of 14 Her, obtained using the LOCI algorithm. North is up and east is to the left. The central $0''.32$ has been masked out since this region is saturated. The stretch is -5σ to 5σ , where σ was computed as the standard deviation in 5 pixel wide ($0''.15$) annuli centered on the star. No candidate companions are identified in the image.

to be 4.76 mag. We used this value and the 14 Her background annulus calculation to determine the contrast as a function of separation from 14 Her. Based on these calculations, we achieve excellent imaging contrast and sensitivity with our observations, reaching contrasts of $\sim 10 \Delta \text{ mag}$ at $0''.4$ and $\gtrsim 13 \Delta \text{ mag}$ beyond $1''$.

3.1. Phase Space Constraints

The true mass of a directly imaged luminous object depends heavily on its age. The younger the host star, the brighter the object is expected to be. Knowing the host star's age accurately is essential for pinning down the companion mass range. Unfortunately, 14 Her's age, like many stars' ages, is fairly uncertain. Kinematically the star is a metal-rich thin-disk star, suggesting an age < 10 Gyr. The chromospheric activity and age-rotation-activity estimates from Mamajek & Hillenbrand (2008) estimate an age of 7.8 Gyr and > 8 Gyr, respectively. Given that 14 Her is very metal-rich ($[\text{Fe}/\text{H}] \sim 0.3$), age-rotation-activity calibrations (as in Mamajek & Hillenbrand 2008) could overestimate the age, since these rely on solar-metallicity calibrator stars. On the other hand, Rocha-Pinto et al. (2000) estimated an age of ~ 3.3 Gyr from chromospheric activity and metallicity studies. However, this value may underestimate the true age since it is based on a linear age-activity fit, which does not appear to accurately fit samples with well-determined ages (Mamajek & Hillenbrand 2008). There are in total seven reported age values of 14 Her. One of these is almost twice the age of the universe (Takeda et al. 2007), so we ignore this value. Because our observational result is a non-detection, we want to quote conservative upper limits to mass and should thus use a conservative age in calculations. Therefore, we take the maximum of the remaining age values⁴ and adopt this value, 8 Gyr, as the age of 14 Her. The COND age tracks do not fall on 8 Gyr, but rather between 5 and 10 Gyr. Therefore, we quote M_J sensitivities interpolated between these two ages.

⁴ 3.33 Gyr (Rocha-Pinto et al. 2000), 5.0 Gyr (Valenti & Fischer 2005), 5.24 Gyr (Takeda 2007), 6.9 Gyr (Wright et al. 2004), 7.8 Gyr (Mamajek & Hillenbrand 2008), and > 8 Gyr (Mamajek & Hillenbrand 2008).

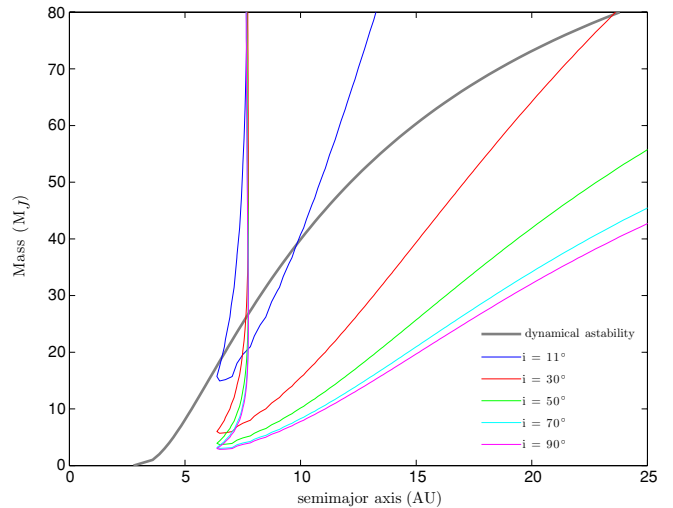


Figure 3. Mass vs. semimajor axis for 14 Her c, from $\Delta\chi^2 = 1$ RV contours (colored lines, $11^\circ < i < 90^\circ$) and an analytic dynamical constraint (gray line). The RV contours were computed by fitting the available RV data from Wittenmyer et al. (2007), Butler et al. (2006), and Naef et al. (2004) at fixed outer planet mass and semimajor axis, allowing all other system parameters to vary. The dynamical constraint, which comes from equations derived by Szebehely & McKenzie (1981), represents the maximum mass 14 Her c could have at a given semimajor axis such that the three-body system is stable.

As a first step toward constraining 14 Her c's phase space, we fit the available RV data from Wittenmyer et al. (2007), Butler et al. (2006), and Naef et al. (2004) at fixed outer planet mass and semimajor axis, allowing all other system parameters to vary. In Figure 3, we plot the $\Delta\chi^2 = 1$ contours for inclination angles ranging from 11° to 90° (colored lines). 14 Her, like most stars with RV planets, has an unknown inclination angle. Nonetheless, Han et al. (2001) found $i > 25^\circ$ and Reffert & Quirrenbach (2011) found $11^\circ < i < 154^\circ$, both using *Hipparcos* astrometry. The latter range is equivalent to $11^\circ < i < 90^\circ$ since we are dealing with the amplitude of $\sin i$. To be conservative, we adopt this range of inclination angles when computing 14 Her c phase space.

A second constraint comes from analytic dynamical analysis. We used equations derived by Szebehely & McKenzie (1981) to calculate the maximum mass 14 Her c could have at a given semimajor axis such that the three-body system is stable. This is shown as the gray curve in Figure 3. The equations assume that both planets have $e = 0$ and treat 14 Her b as a massless test particle. We know that this is not true for 14 Her b; it is both fairly massive ($> 4.64 M_J$) and eccentric ($e = 0.369$), both of which would limit the outer planet's minimum semimajor axis. This means that our results from this analysis are conservative estimates. Any phase space to the left of this dynamical curve is considered unstable.

In addition to ruling out mass and semimajor axis values, the dynamical curve also helps constrain eccentricity. We computed eccentricity contours from the RV fits, but do not plot them (for clarity). The $e > 0.5$ solutions are ruled out since the regions of these eccentricity contours that lie within the $\Delta\chi^2 = 1$ contours correspond to dynamically unstable massive companions. Therefore, we take $e = 0.5$ as an upper limit on 14 Her c's eccentricity.

Constraints from our direct imaging cannot simply be plotted in Figure 3 because this would assume a face-on orientation. For imaging we must deal with projected separation instead of semimajor axis. Therefore, the most probable orbital elements,

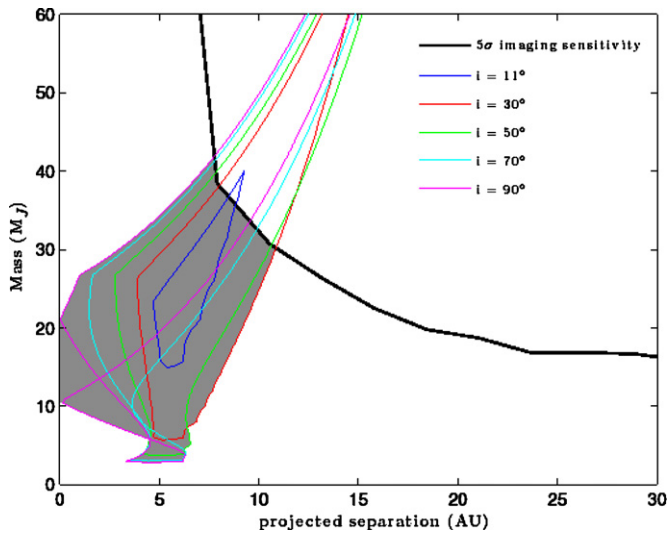


Figure 4. 14 Her c’s mass vs. projected separation at the epoch of our imaging observations. The solid black curve is our imaging sensitivity curve. Any phase space above this line is ruled out at 5σ confidence. The colored contours represent the projected dynamically bound $\Delta\chi^2 = 1$ RV contours. At high inclinations, some orbital solutions place 14 Her c behind or in front of the star due to projection effects. The region shaded gray represents the planet’s most probable mass and separation values.

which are within the regions to the right of the dynamical curve and within the RV contours, must be mapped into projected separation space at the epoch of the imaging observations.

In Figure 4 we plot the dynamically bound RV contours, mapped into projected separation, for $11^\circ < i < 90^\circ$ (colored contours). At high inclinations, some orbital solutions place 14 Her c behind or in front of the star due to projection effects. The final constraint comes from our direct imaging sensitivity (solid black curve in Figure 4). The planet’s allowed mass and separation values must reside below the imaging curve and inside the dynamically bound RV contours. We shade this region gray.

14 Her c then has the following constraint on mass: $3 \lesssim m/M_J \lesssim 42$. Using $42 M_J$ as an upper limit on mass, we can constrain 14 Her c’s semimajor axis. This is shown in Figure 5, which is the same as Figure 3 except that we have included this mass constraint (horizontal black line). The phase space above the horizontal line is ruled out. The allowed phase space, which is below the mass constraint line and to the right of the dynamical curve, is shaded gray. 14 Her c’s semimajor axis is then given by $7 \lesssim a/\text{AU} \lesssim 25$. Our limits agree well with the dynamical results of Goździewski et al. (2008), who estimated a best-fit mass, semimajor axis, and eccentricity of $\sim 8 M_J$, ~ 9 AU, and ~ 0.2 , respectively.

4. CONCLUSIONS: WHAT IS 14 Her c?

A main goal in exoplanet imaging studies is to determine how planets form. Without better constraints on mass, semimajor axis, and eccentricity, we are unable to comment on whether 14 Her c formed by core accretion (Ida & Lin 2004) or disk instability (Boss 1997). However, the close separation and low-mass constraints presented here indicate the object formed out of the disk, rather than via cloud fragmentation. If 14 Her c’s semimajor axis is closer to ~ 7 AU, its mass is likely to be small and comparable to that of 14 Her b, which would suggest formation by core accretion. It may take many more years of additional RV and imaging observations before more powerful

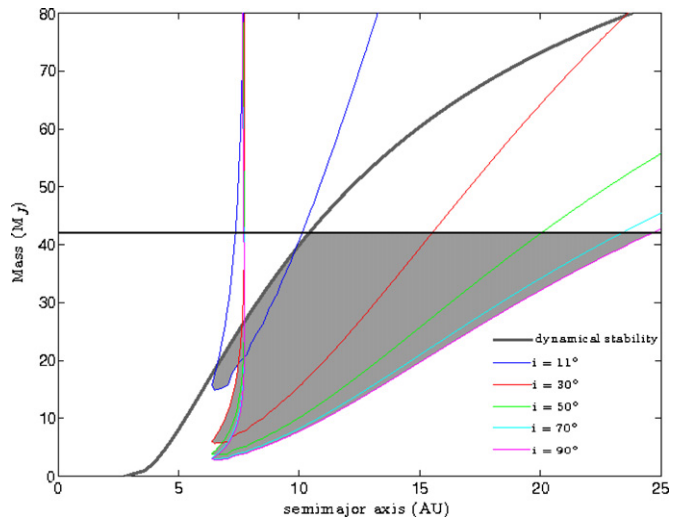


Figure 5. Same as Figure 3, except that the $42 M_J$ upper limit on mass (horizontal black line), which was calculated from Figure 4, is included. The phase space above this line is ruled out. The allowed phase space, which is below this line and to the right of the dynamical curve, is shaded gray. 14 Her c’s maximum semimajor axis is then ~ 25 AU.

constraints can shed light on how the two planets formed. Nonetheless, this work is important for showing the potential of RV/direct imaging overlap. We have demonstrated the “proof of concept,” showing how much orbital phase space can be constrained with just a few hours of observations combined with RV data and simple dynamical analysis. We also showed the importance of considering projected separation of an RV planet when constraining phase space. Future cases of RV/imaging overlap should work in projected separation, as assuming face-on orientations can be misleading. The next generation of large ground- and space-based telescopes will be able to probe lower-mass regimes and will therefore set more powerful constraints. This deeper imaging, combined with continued RV monitoring of systems like 14 Her, will help characterize the architectures of the planetary systems beyond our own.

We thank K. Goździewski and colleagues for sharing their dynamical analysis data. We thank Mike Alegria for operating the telescope and the AO system so smoothly during the observations. We thank the UAO telescope allocation committee for generously providing telescope time for these observations. We thank Eric Nielsen for allowing us to use his orbital element calculator code. We thank the anonymous referee for a very thorough and quickly received referee report. T.J.R. was supported by NASA Headquarters under the NASA Earth and Space Science Fellowship (NESSF) program.

REFERENCES

- Baraffe, I., Chabrier, G., Barman, T. S., Allard, F., & Hauschildt, P. H. 2003, *A&A*, 402, 701
 Boss, A. P. 1997, *Science*, 276, 1836
 Burrows, A., Sudarsky, D., & Lunine, J. I. 2003, *ApJ*, 596, 587
 Butler, R. P., et al. 2006, *ApJ*, 646, 505
 Carson, J. C., Hiner, K. D., Villar, G. G., Blaschak, M. G., Rudolph, A. L., & Stapelfeldt, K. R. 2009, *AJ*, 137, 218
 Currie, T., Bailey, V., Fabrycky, D., Murray-Clay, R., Rodigas, T., & Hinz, P. 2010, *ApJ*, 721, L177
 Freed, M., Hinz, P. M., Meyer, M. R., Milton, N. M., & Lloyd-Hart, M. 2004, *Proc. SPIE*, 5492, 1561
 Goździewski, K., Konacki, M., & Maciejewski, A. J. 2006, *ApJ*, 645, 688
 Goździewski, K., Migaszewski, C., & Konacki, M. 2008, *MNRAS*, 385, 957

- Han, I., Black, D. C., & Gatewood, G. 2001, *ApJ*, **548**, L57
- Heinze, A. N., Hinz, P. M., Kenworthy, M., Miller, D., & Sivanandam, S. 2008, *ApJ*, **688**, 583
- Hinz, P. M., Heinze, A. N., Sivanandam, S., Miller, D. L., Kenworthy, M. A., Brusa, G., Freed, M., & Angel, J. R. P. 2006, *ApJ*, **653**, 1486
- Hinz, P. M., Rodigas, T. J., Kenworthy, M. A., Sivanandam, S., Heinze, A. N., Mamajek, E. E., & Meyer, M. R. 2010, *ApJ*, **716**, 417
- Ida, S., & Lin, D. N. C. 2004, *ApJ*, **616**, 567
- Janson, M., Bergfors, C., Goto, M., Brandner, W., & Lafrenière, D. 2010, *ApJ*, **710**, L35
- Janson, M., et al. 2009, *MNRAS*, **399**, 377
- Kalas, P., et al. 2008, *Science*, **322**, 1345
- Kenworthy, M. A., Mamajek, E. E., Hinz, P. M., Meyer, M. R., Heinze, A. N., Miller, D. L., Sivanandam, S., & Freed, M. 2009, *ApJ*, **697**, 1928
- Lafrenière, D., Marois, C., Doyon, R., Nadeau, D., & Artigau, É. 2007, *ApJ*, **660**, 770
- Lagrange, A., et al. 2009, *A&A*, **493**, L21
- Lagrange, A., et al. 2010, *Science*, **329**, 57
- Leconte, J., et al. 2010, *ApJ*, **716**, 1551
- Leggett, S. K., et al. 2003, *MNRAS*, **345**, 144
- Luhman, K. L., & Jayawardhana, R. 2002, *ApJ*, **566**, 1132
- Mamajek, E. E., & Hillenbrand, L. A. 2008, *ApJ*, **687**, 1264
- Marois, C., Lafrenière, D., Doyon, R., Macintosh, B., & Nadeau, D. 2006, *ApJ*, **641**, 556
- Marois, C., Macintosh, B., Barman, T., Zuckerman, B., Song, I., Patience, J., Lafrenière, D., & Doyon, R. 2008, *Science*, **322**, 1348
- Marois, C., Zuckerman, B., Konopacky, Q. M., Macintosh, B., & Barman, T. 2010, *Nature*, **468**, 1080
- Naef, D., Mayor, M., Beuzit, J. L., Perrier, C., Queloz, D., Sivan, J. P., & Udry, S. 2004, *A&A*, **414**, 351
- Patience, J., et al. 2002, *ApJ*, **581**, 654
- Reffert, S., & Quirrenbach, A. 2011, *A&A*, **527**, A140
- Rocha-Pinto, H. J., Maciel, W. J., Scalo, J., & Flynn, C. 2000, *A&A*, **358**, 850
- Rodigas, T. J., & Hinz, P. M. 2009, *ApJ*, **702**, 716
- Sivanandam, S., Hinz, P. M., Heinze, A. N., Freed, M., & Breuninger, A. H. 2006, *Proc.*, *SPIE*, **6269**
- Szebehely, V., & McKenzie, R. 1981, *Celest. Mech.*, **23**, 3
- Takeda, G., Ford, E. B., Sills, A., Rasio, F. A., Fischer, D. A., & Valenti, J. A. 2007, *ApJS*, **168**, 297
- Takeda, Y. 2007, *PASJ*, **59**, 335
- Thalmann, C., et al. 2009, *ApJ*, **707**, L123
- Valenti, J. A., & Fischer, D. A. 2005, *ApJS*, **159**, 141
- van Leeuwen, F. (ed.) 2007, in *Hipparcos*, the New Reduction of the Raw Data (Astrophys. Space Sci. Lib., Vol. 350; Dordrecht: Springer)
- Wittenmyer, R. A., Endl, M., & Cochran, W. D. 2007, *ApJ*, **654**, 625
- Wright, J. T., Marcy, G. W., Butler, R. P., & Vogt, S. S. 2004, *ApJS*, **152**, 261